ACS APPLIED MATERIALS & INTERFACES

Research Article

www.acsami.org

Effects of Nitrogen Doping on X-band Dielectric Properties of Carbon Nanotube/Polymer Nanocomposites

Mohammad Arjmand and Uttandaraman Sundararaj*

Department of Chemical and Petroleum Engineering, University of Calgary, 2500 University Drive N.W., Calgary, T2N 1N4, Canada

ABSTRACT: Nitrogen-doped and undoped carbon nanotubes (CNTs) were synthesized by selective passing of source and carrier gases (ethane, ammonia, hydrogen, and argon) over an alumina-supported iron catalyst in a quartz tubular reactor at 650 °C. Synthesized CNTs were mixed with polyvinylidene fluoride with an Alberta polymer asymmetric minimixer (APAM) mixer at 240 °C and 235 rpm, and the resulting nanocomposites were compression molded. Transmission electron microscopy (TEM), X-ray photoelectron spectroscopy (XPS), Raman spectroscopy, and thermogravimetric analysis (TGA) techniques revealed that introducing nitrogen into the crystalline structure of CNTs resulted in higher crystalline defects. Dielectric measurements showed that nitrogen doping significantly increased dielectric permittivity for a known dielectric loss. This was ascribed to the role of the crystalline defects and nitrogen atoms, which acted as polarizing centers, blocked the nomadic charges, polarized them, and prevented them from moving along CNTs. The obtained results introduce nitrogen doping as a regulative tool to control the dielectric properties of CNT/polymer nanocomposites.

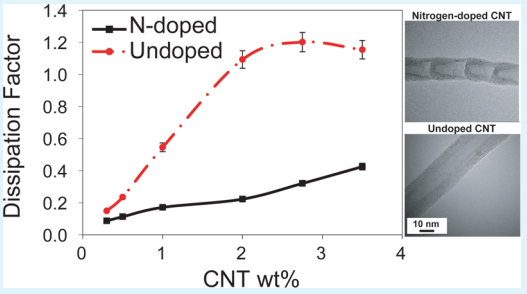

KEYWORDS: *carbon nanotube synthesis, nitrogen doping, dielectric permittivity, charge storage, dielectric loss, polymer nanocomposites*

1. INTRODUCTION

As the electronics industry aims to obtain superior performance, the number of components required within printed circuit boards (PCBs) is increasing. Accordingly, embedding PCB components, such as capacitors, is being suggested as a viable solution to generate advanced PCBs with high integrity. This technology could revolutionize the electronics industry because of advantages such as enhanced PCB integrity, reduction of discrete capacitors, shorter electrical path, electromagnetic interference (EMI) reduction, enhanced CPU speed, lower operation voltage, lower cost, and potential for miniaturization.[1,2]

To develop the technology of embedded capacitors, advanced materials with high permittivity, low loss, lightweight, low cost, and process compatibility with PCBs are desired. Accordingly, conductive filler/polymer composites (CPCs) are being considered as potential constituting materials for embedded capacitors.[3,4] High dielectric permittivity in CPCs arises from the formation of an enormous number of nanocapacitor structures, with conductive filler acting as nanoelectrode and polymer matrix acting as nanodielectric. Nonetheless, as low dissipation is a must for charge storage materials, employing CPCs above the percolation threshold is not possible.[5] Accordingly, maximum dielectric permittivity with an acceptable dielectric loss is only achievable at filler loadings close to and below the percolation threshold, where CPCs are still insulative but have increased dielectric permittivity. In fact, approaching the percolation threshold leads to a reduction in nanodielectric thickness and an increase in the number of nanocapacitors, thereby resulting in enhanced dielectric permittivity.

Essentially, the common technique to tune the dielectric properties of CPCs in the insulative region is to manipulate conductive network formation. To do so, different studies were devoted either to deteriorating conductive network to reduce the leakage current or to raising the percolation threshold to increase the number of nanocapacitors in the insulative region. These techniques include, but are not limited to, incorporating secondary filler as insulative barrier, foaming, employing surface-oxidized metallic nanowire, and aligning carbon nanotubes (CNTs).[6−9] In all these techniques, extra processing on conductive fillers or nanocomposites is required, which is accompanied with some side drawbacks.

Accordingly, the current study introduces the modification of the molecular and crystalline structure of nanofiller, as a novel technique, to tune the dielectric properties of CPCs in the insulative region. CNT was selected as conductive filler because of its rapid industrial growth, high surface area, and extraordinary electrical properties. In this study, nitrogen doping is employed as the tuning tool to control the crystalline structure of CNTs to adjust the dielectric properties of generated nanocomposites. To the best of our knowledge, this work is the first one in the area that employs nitrogen doping to regulate the dielectric properties of CPCs. Nitrogen doping of CNTs was also employed in other technologies such

Received: May 14, 2015
Accepted: July 28, 2015
Published: July 28, 2015

ACS Publications © 2015 American Chemical Society

DOI: 10.1021/acsami.5b04211
ACS Appl. Mater. Interfaces 2015, 7, 17844−17850

as sensing platform for DNA detection, electrocatalysis of hydrogen evolution reaction, and electrocatalysis of oxygen reduction reaction.[10−12]

There are a huge number of studies that discuss the impact of nitrogen doping on the charge-transport properties of CNTs;[13−16] however, there are only a rare number of studies dedicated to the influence of nitrogen doping on the electrical conductivity CNT/polymer nanocomposites, but not dielectric properties.[17] Hence, this study investigates the effect of nitrogen incorporation, and consequently CNT morphology changes, on the X-band (8.2−12.4 GHz) dielectric properties of CNT/polyvinylidene fluoride (PVDF) nanocomposites. The results indicated that nitrogen doping led to an increased number of crystalline defects. These defects together with nitrogen atoms played the role of polarizing centers and significantly improved the dielectric properties.

2. EXPERIMENTAL SECTION

2.1. Materials Preparation. CNTs were synthesized via chemical vapor deposition (CVD) method wherein source and carrier gases were conveyed over an alumina-supported iron catalyst in a quartz tubular reactor with an inner diameter of 4.5 cm. Figure 1 depicts a schematic of the employed CVD setup with all its features. The bubblers were used to absorb the exhaust gases.

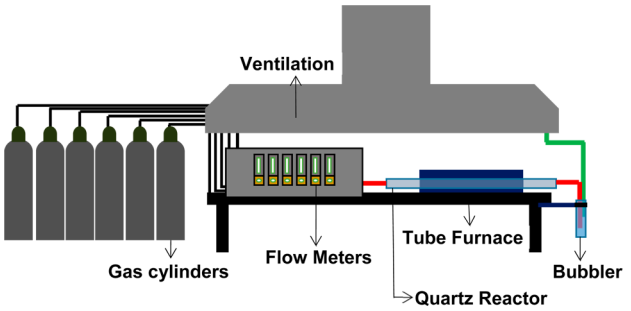

Figure 1. Schematic of employed CVD setup with all its accessories.

The catalyst was prepared by incipient wetness impregnation of iron nitrate (iron(III) nitrate nanohydrate, Baker Analyzed ACS grade) dissolved in water on aluminum oxide support (Sasol Catalox Sba-200), followed by drying, calcination, and reduction. Undoped CNTs were synthesized using a mixture of ethane, hydrogen, and argon. To synthesize nitrogen-doped (N-doped) CNTs, hydrogen gas was replaced with ammonia gas. Ethane was used as the source of carbon, ammonia was the source of nitrogen, and argon and hydrogen were used as gas carriers to keep the reactor free of oxygen during the synthesis process. The synthesis temperature, synthesis time, gas flow rate, and catalyst mass were kept at 650 °C, 2 h, 150 sccm, and 0.6 g, respectively. Further information about the CNT synthesis procedure can be found in our previous studies.[18,19]

A semicrystalline PVDF 11008/0001 was purchased from 3M Canada, with an average density of 1.55 g/cm^3 and a melting point of 160 °C. Synthesized CNTs were mixed with the PVDF matrix using an APAM (Alberta polymer asymmetric minimixer) mixer at 240 °C and 235 rpm The PVDF matrix was first masticated for 3 min, and then CNTs were added and dispersed in the PVDF matrix for an additional 14 min. The samples were prepared at different CNT concentrations, that is, 0.3, 0.5, 1.0, 2.0, 2.7, and 3.5 wt %. A Carver compression molder (Carver Inc., Wabash, IN) was used to make the samples with the dimensions of 24 × 11 × 1.1 mm at 220 °C under 38 MPa pressure for 10 min.

2.2. Materials Characterization. To assess the morphology of CNTs, synthesized CNTs were dispersed into methyl ethyl ketone. The dispersion was treated with low-energy ultrasonic equipment for 3 min, and then one drop of the dispersion was mounted on a copper grid and was dried in air. A transmission electron microscope (Tecnai TF20 G2 FEG-TEM (FEI, Hillsboro, Oregon, USA)) was used to take the images of collected CNTs. Measurement of the length and diameter of CNTs was carried out for 100 individual CNTs for each sample using the ImageJ software. To measure the length of very long nanotubes, several images were stitched together.

A Physical Electronics PHI VersaProbe 5000-XPS was employed to achieve X-ray photoelectron spectroscopy (XPS). The spectra were obtained using a monochromatic Al source at 1486.6 eV and 49.3 W with a beam diameter of 200.0 μm. The samples were pressed on a double-sided tape; a double neutralization was used during spectrum taking, that is, a low-energy electron beam and a low-energy Ar^+ beam were employed. The binding energies were reported relative to C1s at 284.8 eV.

The structural defects of CNTs were investigated using Raman spectroscopy. The powder samples of CNTs were deposited on a clean gold substrate and were analyzed. The Raman spectra were recorded with a Renishaw inVia Raman microscope. Excitation was provided by the radiation of an argon-ion laser with 514 nm wavelength. All spectra were collected with a 5× objective.

The thermal stability of synthesized CNTs was tested using a Thermogravimetric Analyzer TGA (TA Instruments, Q500). The samples were heated under air atmosphere (Praxair AI INDK) from room temperature to 900 °C at a rate of 10 °C/min. The samples were kept at 900 °C for 10 min before cooling.

Dielectric properties measurements in the X-band frequency range were performed using an E5071C network analyzer (ENA series 300 kHz to 20 GHz). The samples were sandwiched between two waveguides of the network analyzer. The network analyzer sent a signal through the waveguide incident to the samples, and then the S-parameters of each sample were recorded and converted to the dielectric properties using Reflection/Transmission Mu and Epsilon method.

3. RESULTS AND DISCUSSION

3.1. Transmission Electron Microscopy. Figure 2 depicts the TEM micrographs of synthesized CNTs at two various magnifications. The TEM micrographs revealed that N-doped CNTs had bamboo-like structure, which differed from open-channel undoped CNTs. It is also clearly seen that the wall of N-doped CNTs is thicker in the straight region than in the disordered region. This leads to surface roughness in N-doped CNTs, which arises from the flawed linkage of the bamboo-like compartments.

The high magnification TEM images demonstrate the presence of highly defective areas in N-doped CNTs, indicated by arrows. This can be ascribed to nitrogen decorations into the molecular structure of CNTs leading to local distortions within the graphitic structure of CNTs. On the other hand, undoped CNTs show an open-channel structure with a well-ordered, less-defective wall structure.

It has been proposed that nitrogen may enhance bamboo-like structure formation.[20,21] Nevertheless, Chizari and Sundararaj[19] and van Dommele et al.[22] observed that N-doped CNTs grown over Fe catalysts had bamboo-like structures whereas the ones grown over Co catalyst, despite having nitrogen bonding, were mostly open-channel. Thus, it seems improbable that only nitrogen doping causes bamboo-like structure. According to van Dommele et al.,[23] the probability of the formation of graphitic envelope around Fe is higher than around Co, and thus, CNTs grown over Fe catalyst are more probable to form bamboo-like configuration.

As shown in Figure 3, the average diameters of N-doped and undoped CNTs were 49 and 15 nm, respectively. Measuring the diameters of catalyst particles showed that there is a good correlation between CNT diameter and catalyst size distribu-

DOI: 10.1021/acsami.5b04211
ACS Appl. Mater. Interfaces 2015, 7, 17844−17850

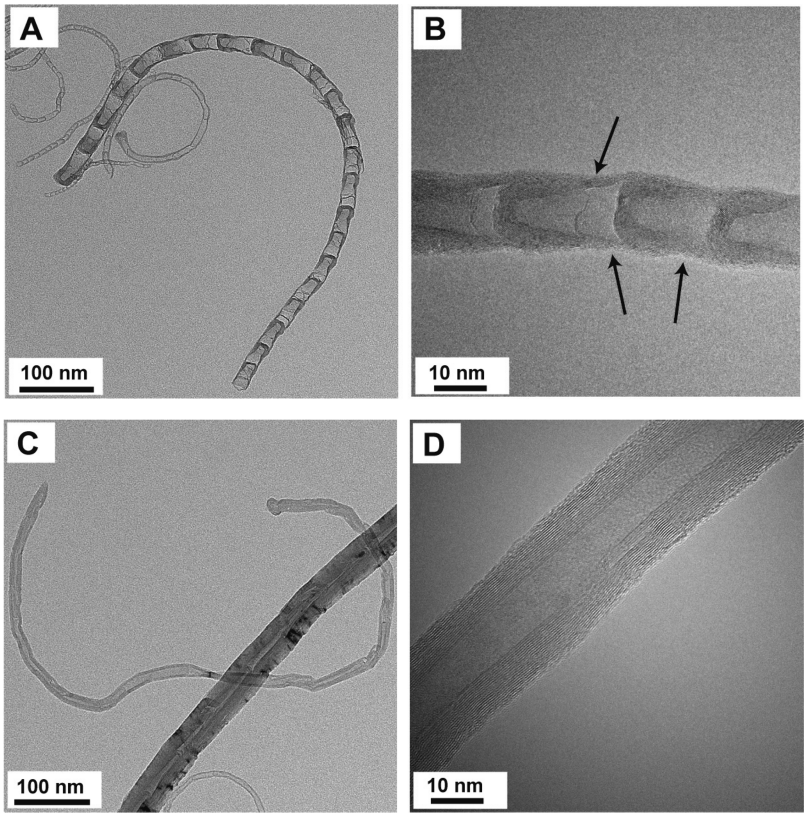

Figure 2. TEM micrographs of N-doped CNTs (A and B) and undoped CNTs (C and D) at various magnifications.

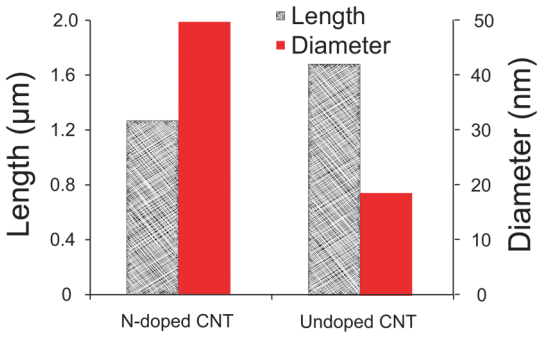

Figure 3. Average length and diameter of N-doped and undoped CNTs synthesized over alumina-supported iron catalyst.

tion. This correlation was also observed by other studies.[24,25] The variation in the particle size of the growth catalysts can be ascribed to differences in catalyst size both before and after the synthesis. Thermal decomposition of the precursor molecules combined with high reaction temperature results in sintering, or liquefaction and coalescence, of the catalyst particles.[26] Thus, different types of synthesis gases (hydrogen versus ammonia) could account for dissimilar catalyst size distributions.

It was also observed that the average length of N-doped CNTs (1.3 μm) was smaller than that of undoped ones (1.7 μm). This difference can be attributed to the presence of nitrogen in the crystalline structure of N-doped CNTs, which led to more disordered and capped structure, thereby restricting the growth of N-doped CNTs. The higher length of undoped CNTs can also be attributed to the fact that the majority of undoped CNTs were open-channel, which means that most of the carbon atoms participated in increasing the length of undoped CNTs.

3.2. CNT Structure and Crystallinity. Essentially, there are three common nitrogen bonding configurations in N-doped CNTs, namely, quaternary, pyridinic, and pyrrolic. As shown in Figure 4a, quaternary nitrogen is directly substituted for a C atom in the hexagonal network, is sp^2 hybridized, and generates electron-donor state. The pyridinic nitrogen type is a member of six-fold ring arrangement, is sp^2 hybridized, and has a lone pair, which enters a nonbonding orbital. Pyrrolic nitrogen is a part of a five-membered ring structure, is sp^3 hybridized, and donates its remaining two electrons to a π orbital, completing the aromatic ring.[27] While the quaternary and pyridinic bondings cause side-wall defects, the pyrrolic moieties are believed to account for internal cappings creating bamboo-like compartments.[22,28] A fourth type has been reported and labeled as N−X species, which is believed to be an oxidized type of pyridinic nitrogen. Nitrogen may also bond as nitrile and amine or exist as N_2 intercalated between nanotubes.[29]

The nitrogen types in N-doped CNTs can be distinguished by employing XPS technique. As shown in Figure 4b, XPS peaks correspond to pyridinic nitrogen (398.3−399.8 eV), pyrrolic nitrogen (400.1−400.5 eV), quaternary nitrogen (401−401.4 eV), and nitrogen oxide species or trapped N_2 molecules (404−405.6 eV).[19,30,31] The XPS results disclosed that nitrogen/carbon atomic percentage in N-doped CNT was 3.85 at. % and that the percentages of quaternary, pyridinic, pyrrolic, and N−X bonding were 29.3, 26.4, 5.2, and 39.1, respectively (Figure 4c).

The physicochemical properties of N-doped CNTs depend on both nitrogen content and type of nitrogen bonding. A higher amount of nitrogen leads to more crystalline defects, and the various types of nitrogen incorporation affect the electronic properties of N-doped CNTs differently. Zhong et al.[15] and

DOI: 10.1021/acsami.5b04211
ACS Appl. Mater. Interfaces 2015, 7, 17844−17850

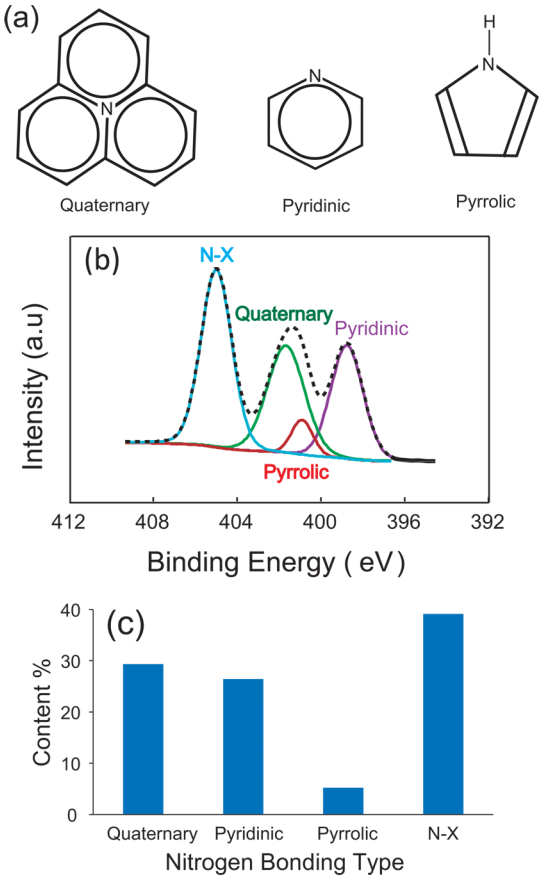

Figure 4. (a) Major types of nitrogen bonding in N-doped CNTs, (b) XPS N1s spectra of N-doped CNTs, and (c) graph of percentage of different types of nitrogen incorporation in N-doped CNTs.

Ghosh et al.[16] claimed that quaternary nitrogen increases the electronic density of states at the doping site and, hence, improves the electronic conductivity, whereas pyridinic dopant behaves in a reverse manner and destroys the sublevels of unoccupied states near the Fermi level. Nonetheless, in other studies, Choi et al.[31] and Czerw et al.[13] asserted that pyridinic nitrogen induces metallic behavior.

Raman spectroscopy provides critical information about the structural defects in CNTs. The incorporation of dopants, such as nitrogen, in CNTs has shown to create defects, which can be tracked by Raman spectroscopy. Two significant characteristics in the Raman spectra of CNTs are D band (disorder band) and G band (graphite band). The D band (around 1400 cm^{-1}) corresponds to disorders in sp^2 hybridized graphitic structure, while the G band (around 1600 cm^{-1}) arises from C−C stretching in sp^2 carbon network and is observed in all the Raman spectra of graphitic carbon.[32,33]

The ratio of the D and G bands intensities (I_D/I_G) is often used as a diagnostic tool for assessing the crystallinity of CNTs. The Raman spectra (Figure 5) showed that the ratios I_D/I_G for N-doped and undoped CNTs were 0.82 and 0.66, respectively. These data confirm that nitrogen doping increased the number of defects in the CNT structure. In line with the current study, Villalpando-Paez et al.[34] and Ibrahim et al.[35] observed a direct relationship between nitrogen concentration and the I_D/I_G ratio. The pyridinic type of nitrogen is suggested to be the main contributor to the disturbance of CNT walls.[36] These disturbances can emerge as pentagons, heptagons, or

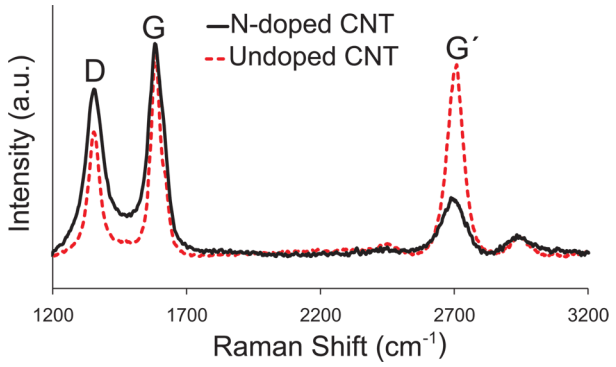

Figure 5. Raman spectra of N-doped and undoped CNTs.

replacement of nitrogen in the hexagonal carbon rings, which result in changes in the electronic properties of CNTs.

All kinds of sp^2 materials present an intense Raman feature in the range of 2500−2800 cm^{-1}, called G′ band, which is sensitive to changes in the electronic structure of the graphitic layers.[33] As the incorporation of dopant alters the electronic structure, the intensity of G′ band can be employed as a strong tool to estimate the degree of doping in CNTs.[32,37] As depicted in Figure 5, the intensity of G′ dropped drastically after nitrogen doping of CNTs, signifying the impact of doping on the electronic structure of CNTs. This is well in agreement with the study performed by Bulusheva et al.[32] who reported a strong reduction in the G′ band intensity of CNTs after nitrogen doping.

Kim et al.[38] demonstrated that G′ band intensity can be used as a measure of metallicity in CNTs. They observed that metallic CNTs showed higher $I_{G'}/I_G$ ratio than semiconducting CNTs. It was also reported that the G′ band had a high intensity for highly ordered pyrolitic graphite characterized by negligible intensity of the D band.[33,39] Thus, the $I_{G'}/I_G$ ratio could be considered as a criterion for the metallicity of synthesized N-doped CNTs.

Thermal stability of synthesized CNTs was investigated using thermogravimetric analysis (TGA) in air atmosphere. It is believed that structural defects in the crystalline structure of CNTs act as weak points and deteriorate thermal stability of CNTs.[40,41] Figure 6 shows that the inflection points for N-

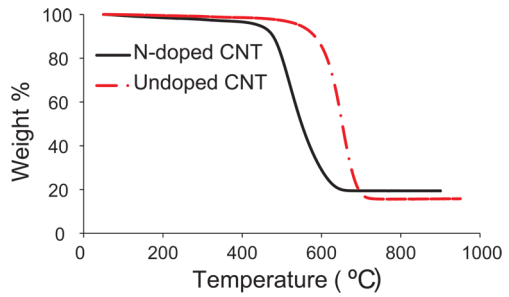

Figure 6. TGA analysis of N-doped and undoped CNTs in air atmosphere.

doped and undoped CNTs were 517 and 650 °C, respectively. Thus, it can be inferred that N-doped CNTs possess inferior crystalline structure, which makes them more susceptible to thermal degradation.

Dispersion and distribution of conductive fillers within the polymer matrix are highly influential on the final electrical

DOI: 10.1021/acsami.5b04211
ACS Appl. Mater. Interfaces 2015, 7, 17844−17850

properties of CPCs.[42−44] Hence, we performed optical microscopy and transmission electron microscopy to detect any discrepancy in the dispersion and distribution states of CNTs in the generated nanocomposites. Our observations showed very similar states of dispersion and distribution for all the samples. Therefore, we believe that the difference in the dielectric properties of the generated CPCs did originate from discrepancies in the physical and structural properties of synthesized CNTs, that is, diameter, length, nitrogen content, nitrogen bonding type, and crystalline structure.

3.3. Impact of Nitrogen Doping on X-band Dielectric Properties. Increasing dielectric permittivity in CPCs is performed by raising filler content, which is unfavorably accompanied by higher dielectric loss; hence, CPCs are restricted to be in the insulative region. Accordingly, manipulating the molecular structure of conductive filler could be employed as an efficient route to increase the dielectric permittivity in the insulative region.

As verified by Raman spectroscopy and TGA analysis, N-doped CNTs had inferior crystallinity and greater number of structural defects relative to undoped ones. Given that structural defects and nitrogen atoms can act as polarization centers, nitrogen doping could be used as a tool to manipulate the dielectric properties of CNT/polymer nanocomposites. To verify this, the dielectric properties of the N-doped and undoped CNT/PVDF nanocomposites were compared with each other (Figure 7). Interestingly, both dielectric permittivity

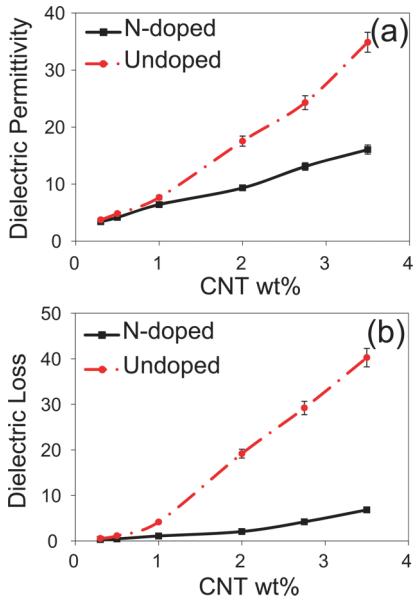

Figure 7. (a) Dielectric permittivity and (b) dielectric loss of N-doped and undoped nanocomposites as a function of CNT content.

and dielectric loss of the N-doped nanocomposites were lower than those of the undoped ones, and the discrepancy was much more evident at high filler loadings.

Dielectric permittivity in CNT/PVDF nanocomposites over the X-band primarily originates from the space polarization within CNTs in combination with the electronic polarization of the PVDF matrix. Other polarization mechanisms, such as interfacial and dipolar, diminish over the X-band because of relaxation phenomena.[45,46] Dielectric loss in CNT/polymer nanocomposites comprises two components, that is, Ohmic loss and polarization loss. Ohmic loss represents the dissipation of electrical energy by nomadic charges moving throughout the dielectric material; polarization loss arises from the dissipation of energy to overcome the momentum to reorient dipoles in each half cycle of alternating field.[47−49]

Essentially, two chief factors contribute to the dielectric permittivity of CNTs, namely, (1) the amount of nomadic charges that participate in space charge polarization (metallicity) and (2) the number of polarization centers. The magnitude of an electric dipole is proportional to the amount of polarized charges, and thus, a greater number of nomadic charges corresponds to larger space polarization within CNTs. On the other hand, a larger amount of structural defects signifies a larger number of polarization centers. As confirmed by Raman spectroscopy and TGA analysis, undoped CNTs had higher crystallinity, metallicity, and thus a larger number of nomadic charges but a lower number of structural defects. Given the higher dielectric permittivity of the undoped nanocomposites, we claim that the impact of higher metallicity (larger number of nomadic charges) overshadowed the smaller number of polarization centers in undoped CNTs and, hence, resulted in higher dielectric permittivity compared to N-doped CNTs. Moreover, a larger number of nomadic charges generates greater applied electric field within nanocapacitors, thereby leading to boosted PVDF electronic polarization.

Three major reasons account for higher dielectric loss in undoped CNTs: (1) greater number of dissipative nomadic charges, (2) enhanced conductive network formation, and (3) lower number of scattering centers (structural defects and nitrogen atoms). Enhanced conductive network corresponds to prolonged free paths for electrons to go through in each half cycle of alternating field and, thus, higher dissipation of electrical energy.[49] Likewise, a lower number of scattering centers signifies longer electrons' mean free paths.[35,50] For N-doped CNTs, inferior conductive network (due to lower aspect ratio), poorer crystallinity, and metallicity (as confirmed by Raman spectroscopy), and the presence of nitrogen can justify their lower dielectric loss.

So far, it was observed that nitrogen doping decreased the dielectric loss favorably, whereas it also had an adverse influence on the dielectric permittivity. Thus, to assess the overall impact of nitrogen doping on the dielectric properties, the dissipation factors tan δ (dielectric loss/dielectric permittivity) of the N-doped and the undoped nanocomposites were compared with each other. As shown in Figure 8, it was observed that nitrogen doping reduced the dissipation factor of the CNT/PVDF nanocomposites significantly. This confirms the positive impact of nitrogen doping on the dielectric properties.

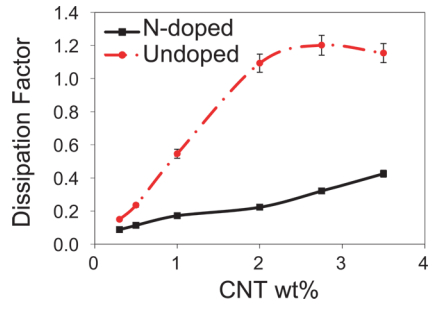

Figure 8. Dissipation factor of N-doped and undoped nanocomposites as a function of CNT content.

DOI: 10.1021/acsami.5b04211
ACS Appl. Mater. Interfaces 2015, 7, 17844−17850

For instance, for the 2.0 wt % CNT/PVDF nanocomposites, the dissipation factor of the N-doped nanocomposites was 0.22, which was 5 times less than the undoped ones. In another scenario, for a dielectric permittivity equal to 9.0, the N-doped and undoped nanocomposites showed the dielectric loss of 1.96 and 6.21, respectively. The N-doped nanocomposites, because of inferior CNT crystallinity, required a larger amount of CNTs to present any dielectric permittivity. These results propose nitrogen doping as a promising technique to regulate the dielectric properties of CNT/polymer nanocomposites. We believe that the structural defects and nitrogen atoms in N-doped CNTs played the role of polarizing centers and thus contributed to the dielectric permittivity. In fact, polarization centers blocked nomadic charges, polarized them, and prevented them from moving along CNTs.

4. CONCLUSIONS

This study introduced nitrogen doping as a promising technique to improve the dielectric properties of CNT/polymer nanocomposites. As confirmed by XPS, Raman spectroscopy, and TGA analysis, nitrogen was incorporated into the crystalline structure of CNTs as various types, that is, quaternary, pyridinic, and pyrrolic, and resulted in higher crystalline defects, that is, inferior crystalline structure of CNTs.

It was observed that the N-doped nanocomposites showed lower dielectric permittivity and dielectric loss relative to the undoped nanocomposites. These were attributed to poorer crystalline structure, lower number of nomadic charges, and lower aspect ratio of N-doped CNTs. To be more precise, nitrogen doping had a positive effect of lowering the dielectric loss, which significantly overshadowed its negative impact on reducing the dielectric permittivity. In fact, although the number of nomadic charges participating in charge polarization decreased because of poorer crystallinity, the role of structural defects and nitrogen atoms acting as polarizing centers dominated and improved the dielectric properties. Therefore, it can be inferred that nitrogen doping can be used as an efficient technique to manipulate the dielectric properties of CNT/polymer nanocomposites.

AUTHOR INFORMATION

Corresponding Author

*Tel: +1 403 2106549. E-mail: u.sundararaj@ucalgary.ca.

Notes

The authors declare no competing financial interest.

ACKNOWLEDGMENTS

Financial support from the Natural Sciences and Engineering Research Council (NSERC) of Canada is highly appreciated. We would like to gratefully acknowledge Dr. Kambiz Chizari and Messrs. Alexander Vena and Tarik Naif Abdalla for their assistance with the carbon nanotube synthesis and nanocomposites preparation. We would like to thank Dr. Lars Laurentius for his great assistance with Raman spectroscopy.

REFERENCES

(1) Vardaman, E. J.; Matthew, L. C.; Carpenter, K. Market Drivers for Embedded Components Packaging. www.techsearchinc.com:http://www.semi.org/eu/sites/semi.org/files/docs/VardamanEmbMktHD.pdf, (accessed Apr 15, 2015).

(2) Andresakis, J. Reduction of Discrete Capacitors Using Embedded Capacitance Layers: Simulation versus Actual Results. www.oakmitsui.com, (accessed Apr 15, 2015).

(3) Ameli, A.; Nofar, M.; Park, C. B.; Potschke, P.; Rizvi, G. Polypropylene/Carbon Nanotube Nano/Microcellular Structures with High Dielectric Permittivity, Low Dielectric Loss, and Low Percolation Threshold. *Carbon* **2014**, *71*, 206−217.

(4) Li, J. J.; Seok, S. I.; Chu, B. J.; Dogan, F.; Zhang, Q. M.; Wang, Q. Nanocomposites of Ferroelectric Polymers with TiO_2 Nanoparticles Exhibiting Significantly Enhanced Electrical Energy Density. *Adv. Mater.* **2009**, *21* (2), 217−221.

(5) Jiang, M. J.; Dang, Z. M.; Bozlar, M.; Miomandre, F.; Bai, J. B. Broad-Frequency Dielectric Behaviors in Multiwalled Carbon Nanotube/Rubber Nanocomposites. *J. Appl. Phys.* **2009**, *106* (8), 084902 (1−6).

(6) Arjmand, M.; Sundararaj, U. Impact of BaTiO3 as Insulative Ferroelectric Barrier on the Broadband Dielectric Properties of MWCNT/PVDF Nanocomposites. *Polym. Compos.* **2014**, n/a.

(7) Arjmand, M.; Mahmoodi, M.; Park, S.; Sundararaj, U. Impact of Foaming on the Broadband Dielectric Properties of Multi-walled Carbon Nanotube/Polystyrene Composites. *J. Cell. Plast.* **2014**, *50* (6), 551−562.

(8) da Silva, A. B.; Arjmand, M.; Sundararaj, U.; Bretas, R. E. S. Novel Composites of Copper Nanowire/PVDF with Superior Dielectric Properties. *Polymer* **2014**, *55* (1), 226−234.

(9) Arjmand, M.; Mahmoodi, M.; Park, S.; Sundararaj, U. An Innovative Method to Reduce the Energy Loss of Conductive Filler/Polymer Composites for Charge Storage Applications. *Compos. Sci. Technol.* **2013**, *78*, 24−29.

(10) Liu, Q.; Pu, Z.; Asiri, A. M.; Sun, X. Bamboo-like Nitrogen-doped Carbon Nanotubes toward Fluorescence Recovery Assay for DNA Detection. *Sens. Actuators, B* **2015**, *206*, 37−42.

(11) Liu, Q.; Pu, Z.; Asiri, A. M.; Sun, X. Nitrogen-doped Carbon Nanotube Supported Iron Phosphide Nanocomposites for Highly Active Electrocatalysis of the Hydrogen Evolution Reaction. *Electrochim. Acta* **2014**, *149*, 324−329.

(12) Liu, Q.; Pu, Z.; Tang, C.; Asiri, A. M.; Qusti, A. H.; Al-Youbi, A. O.; Sun, X. N-doped carbon nanotubes from functional tubular polypyrrole: A Highly Efficient Electrocatalyst for Oxygen Reduction Reaction. *Electrochem. Commun.* **2013**, *36*, 57−61.

(13) Czerw, R.; Terrones, M.; Charlier, J. C.; Blase, X.; Foley, B.; Kamalakaran, R.; Grobert, N.; Terrones, H.; Tekleab, D.; Ajayan, P. M.; Blau, W.; Ruhle, M.; Carroll, D. L. Identification of Electron Donor States in N-doped Carbon Nanotubes. *Nano Lett.* **2001**, *1* (9), 457−460.

(14) Wiggins-Camacho, J. D.; Stevenson, K. J. Effect of Nitrogen Concentration on Capacitance, Density of States, Electronic Conductivity, and Morphology of N-Doped Carbon Nanotube Electrodes. *J. Phys. Chem. C* **2009**, *113* (44), 19082−19090.

(15) Zhong, Z.; Lee, G. I.; Bin Mo, C.; Hong, S. H.; Kang, J. K. Tailored Field-Emission Property of Patterned Carbon Nitride Nanotubes by a Selective Doping of Substitutional N(sN) and Pyridine-like N(pN) Atoms. *Chem. Mater.* **2007**, *19* (12), 2918−2920.

(16) Ghosh, K.; Kumar, M.; Maruyama, T.; Ando, Y. Tailoring the Field Emission Property of Nitrogen-doped Carbon Nanotubes by Controlling the Graphitic/Pyridinic Substitution. *Carbon* **2010**, *48* (1), 191−200.

(17) Kanygin, M. A.; Sedelnikova, O. V.; Asanov, I. P.; Bulusheva, L. G.; Okotrub, A. V.; Kuzhir, P. P.; Plyushch, A. O.; Maksimenko, S. A.; Lapko, K. N.; Sokol, A. A.; Ivashkevich, O. A.; Lambin, P. Effect of Nitrogen Doping on the Electromagnetic Properties of Carbon Nanotube-based Composites. *J. Appl. Phys.* **2013**, *113* (14), 144315 (1−8).

(18) Chizari, K.; Vena, A.; Laureritius, L.; Sundararaj, U. The Effect of Temperature on the Morphology and Chemical Surface Properties of Nitrogen-doped Carbon Nanotubes. *Carbon* **2014**, *68*, 369−379.

(19) Chizari, K.; Sundararaj, U. The Effects of Catalyst on the Morphology and Physicochemical Properties of Nitrogen-doped Carbon Nanotubes. *Mater. Lett.* **2014**, *116*, 289−292.

(20) Lin, C. H.; Chang, H. L.; Hsu, C. M.; Lo, A. Y.; Kuo, C. T. The Role of Nitrogen in Carbon Nanotube Formation. *Diamond Relat. Mater.* **2003**, *12* (10−11), 1851−1857.

DOI: 10.1021/acsami.5b04211
ACS Appl. Mater. Interfaces 2015, 7, 17844−17850

(21) Chang, H. L.; Lin, C. H.; Kuo, C. T. Field Emission, Structure, Cathodoluminescence and Formation Studies of Carbon and Si-C-N Nanotubes. *Diamond Relat. Mater.* **2002**, *11* (3−6), 793−798.
(22) van Dommele, S.; Romero-Izquirdo, A.; Brydson, R.; de Jong, K. P.; Bitter, J. H. Tuning Nitrogen Functionalities in Catalytically Grown Nitrogen-containing Carbon Nanotubes. *Carbon* **2008**, *46* (1), 138−148.
(23) van Dommele, S.; de Jong, K. P.; Romero-Izquirdo, A.; Bitter, J. H. Synthesis of Heterogeneous Base Catalysts: Nitrogen Containing Carbon Nanotubes. *Scientific Bases for the Preparation of Heterogeneous Catalysts*, Proceedings of the 9th International Symposium, Louvain-la-Neuve, Belgium, 2006; Vol. *162*, pp 29−36.10.1016/S0167-2991(06)80887-6
(24) Lee, C. J.; Park, J.; Yu, J. A. Catalyst Effect on Carbon Nanotubes Synthesized by Thermal Chemical Vapor Deposition. *Chem. Phys. Lett.* **2002**, *360* (3−4), 250−255.
(25) Alvarez, W. E.; Kitiyanan, B.; Borgna, A.; Resasco, D. E. Synergism of Co and Mo in the Catalytic Production of Single-wall Carbon Nanotubes by Decomposition of CO. *Carbon* **2001**, *39* (4), 547−558.
(26) Moisala, A.; Nasibulin, A. G.; Kauppinen, E. I. The Role of Metal Nanoparticles in the Catalytic Production of Single-walled Carbon Nanotubes - a Review. *J. Phys.: Condens. Matter* **2003**, *15* (42), S3011−S3035.
(27) Sharifi, T.; Hu, G.; Jia, X.; Wagberg, T. Formation of Active Sites for Oxygen Reduction Reactions by Transformation of Nitrogen Functionalities in Nitrogen-Doped Carbon Nanotubes. *ACS Nano* **2012**, *6* (10), 8904−8912.
(28) Pels, J. R.; Kapteijn, F.; Moulijn, J. A.; Zhu, Q.; Thomas, K. M. Evolution of Nitrogen Functionalities in Carbonaceous Materials during Pyrolysis. *Carbon* **1995**, *33* (11), 1641−1653.
(29) Burch, H. J. Bioapplications of Nitrogen Doped Carbon Nanotubes. Ph.D. Thesis, University of Oxford, U.K., 2006.
(30) Kudashov, A. G.; Okotrub, A. V.; Bulusheva, L. G.; Asanov, L. P.; Shubin, Y. V.; Yudanov, N. F.; Yudanova, L. I.; Danilovich, V. S.; Abrosimov, O. G. Influence of Ni-Co Catalyst Composition on Nitrogen Content in Carbon Nanotubes. *J. Phys. Chem. B* **2004**, *108* (26), 9048−9053.
(31) Choi, H. C.; Park, J.; Kim, B. Distribution and Structure of N Atoms in Multiwalled Carbon Nanotubes using Variable-Energy X-ray Photoelectron Spectroscopy. *J. Phys. Chem. B* **2005**, *109* (10), 4333−4340.
(32) Bulusheva, L. G.; Okotrub, A. V.; Kinloch, I. A.; Asanov, I. P.; Kurenya, A. G.; Kudashov, A. G.; Chen, X.; Song, H. Effect of Nitrogen Doping on Raman Spectra of Multi-walled Carbon Nanotubes. *Phys. Status Solidi B* **2008**, *245* (10), 1971−1974.
(33) Dresselhaus, M. S.; Jorio, A.; Hofmann, M.; Dresselhaus, G.; Saito, R. Perspectives on Carbon Nanotubes and Graphene Raman Spectroscopy. *Nano Lett.* **2010**, *10* (3), 751−758.
(34) Villalpando-Paez, F.; Zamudio, A.; Elias, A. L.; Son, H.; Barros, E. B.; Chou, S. G.; Kim, Y. A.; Muramatsu, H.; Hayashi, T.; Kong, J.; Terrones, H.; Dresselhaus, G.; Endo, M.; Terrones, M.; Dresselhaus, M. S. Synthesis and Characterization of Long Strands of Nitrogen-doped Single-walled Carbon Nanotubes. *Chem. Phys. Lett.* **2006**, *424* (4−6), 345−352.
(35) Ibrahim, E. M. M.; Khavrus, V. O.; Leonhardt, A.; Hampel, S.; Oswald, S.; Rummeli, M. H.; Buchner, B. Synthesis, Characterization, and Electrical Properties of Nitrogen-doped Single-walled Carbon Nanotubes with Different Nitrogen Content. *Diamond Relat. Mater.* **2010**, *19* (10), 1199−1206.
(36) Liu, J. W.; Webster, S.; Carroll, D. L. Temperature and Flow Rate of NH3 Effects on Nitrogen Content and Doping Environments of Carbon Nanotubes Grown by Injection CVD Method. *J. Phys. Chem. B* **2005**, *109* (33), 15769−15774.
(37) Maciel, I. O.; Anderson, N.; Pimenta, M. A.; Hartschuh, A.; Qian, H. H.; Terrones, M.; Terrones, H.; Campos-Delgado, J.; Rao, A. M.; Novotny, L.; Jorio, A. Electron and Phonon Renormalization Near Charged Defects in Carbon Nanotubes. *Nat. Mater.* **2008**, *7* (11), 878−883.
(38) Kim, K. K.; Park, J. S.; Kim, S. J.; Geng, H. Z.; An, K. H.; Yang, C. M.; Sato, K.; Saito, R.; Lee, Y. H. Dependence of Raman Spectra G′ Band Intensity on Metallicity of Single-wall Carbon Nanotubes. *Phys. Rev. B: Condens. Matter Mater. Phys.* **2007**, *76*, 20.
(39) Antunes, E. F.; Lobo, A. O.; Corat, E. J.; Trava-Airoldi, V. J.; Martin, A. A.; Verissimo, C. Comparative Study of First- and Second-order Raman Spectra of MWCNT at Visible and Infrared Laser Excitation. *Carbon* **2006**, *44* (11), 2202−2211.
(40) Li, H. P.; Zhao, N. Q.; He, C. N.; Shi, C. S.; Du, X. W.; Li, H. J. Thermogravimetric Analysis and TEM Characterization of the Oxidation and Defect Sites of Carbon Nanotubes Synthesized by CVD of Methane. *Mater. Sci. Eng., A* **2008**, *473* (1−2), 355−359.
(41) Bom, D.; Andrews, R.; Jacques, D.; Anthony, J.; Chen, B. L.; Meier, M. S.; Selegue, J. P. Thermogravimetric Analysis of the Oxidation of Multiwalled Carbon Nanotubes: Evidence for the Role of Defect Sites in Carbon Nanotube Chemistry. *Nano Lett.* **2002**, *2* (6), 615−619.
(42) Ke, K.; Pötschke, P.; Jehnichen, D.; Fischer, D.; Voit, B. Achieving β-phase poly(vinylidene fluoride) from melt cooling: Effect of surface functionalized carbon nanotubes. *Polymer* **2014**, *55* (2), 611−619.
(43) Li, J.; Ma, P. C.; Chow, W. S.; To, C. K.; Tang, B. Z.; Kim, J. K. Correlations between percolation threshold, dispersion state, and aspect ratio of carbon nanotubes. *Adv. Funct. Mater.* **2007**, *17* (16), 3207−3215.
(44) TabkhPaz, M.; Mahmoodi, M.; Arjmand, M.; Sundararaj, U.; Chu, J.; Park, S. S. Investigation of Chaotic Mixing for MWCNT/Polymer Composites. *Macromol. Mater. Eng.* **2015**, *300* (5), 482−496.
(45) Dang, Z. M.; Yuan, J. K.; Zha, J. W.; Zhou, T.; Li, S. T.; Hu, G. H. Fundamentals, Processes and Applications of High-permittivity Polymer Matrix Composites. *Prog. Mater. Sci.* **2012**, *57* (4), 660−723.
(46) Yao, S. H.; Dang, Z. M.; Jiang, M. J.; Bai, J. B. $BaTiO_3$-Carbon Nanotube/Polyvinylidene Fluoride Three-Phase Composites with High Dielectric Constant and Low Dielectric Loss. *Appl. Phys. Lett.* **2008**, *93* (18), 182905 (1−4).
(47) Arjmand, M.; Apperley, T.; Okoniewski, M.; Sundararaj, U. Comparative Study of Electromagnetic Interference Shielding Properties of Injection Molded versus Compression Molded Multi-walled Carbon Nanotube/Polystyrene Composites. *Carbon* **2012**, *50* (14), 5126−5134.
(48) Huang, Y.; Li, N.; Ma, Y. F.; Feng, D.; Li, F. F.; He, X. B.; Lin, X.; Gao, H. J.; Chen, Y. S. The Influence of Single-walled Carbon Nanotube Structure on the Electromagnetic Interference Shielding Efficiency of Its Epoxy Composites. *Carbon* **2007**, *45* (8), 1614−1621.
(49) Arjmand, M.; Moud, A. A.; Li, Y.; Sundararaj, U. Outstanding Electromagnetic Interference Shielding of Silver Nanowires: Comparison with Carbon Nanotubes. *RSC Adv.* **2015**, *5* (70), 56590−56598.
(50) Latil, S.; Roche, S.; Mayou, D.; Charlier, J. C. Mesoscopic Transport in Chemically Doped Carbon Nanotubes. *Phys. Rev. Lett.* **2004**, *92* (25), 4.

DOI: 10.1021/acsami.5b04211
ACS Appl. Mater. Interfaces 2015, 7, 17844−17850